inorganics

MDPI

Article

On the Structural and Vibrational Properties of Solid Endohedral Metallofullerene Li@C_{60}

Martina Vrankić [1,†], Takeshi Nakagawa [2,†], Melita Menelaou [3,†], Yasuhiro Takabayashi [4,†], Naoya Yoshikane [5], Keisuke Matsui [6], Ken Kokubo [7,‡], Kenichi Kato [8], Saori Kawaguchi-Imada [9], Hirokazu Kadobayashi [9], John Arvanitidis [10], Yoshiki Kubota [5] and Kosmas Prassides [5,11,*]

1 Division of Materials Physics, Ruđer Bošković Institute, 10000 Zagreb, Croatia
2 Center for High-Pressure Science & Technology Advanced Research, Beijing 100094, China
3 Department of Mechanical Engineering and Materials Science and Engineering, Cyprus University of Technology, Limassol 3036, Cyprus
4 Department of Physical Science and Engineering, Nagoya Institute of Technology, Nagoya 466-8555, Japan
5 Department of Physics, Graduate School of Science, Osaka Metropolitan University, Osaka 599-8531, Japan
6 Department of Materials Science, Graduate School of Engineering, Osaka Metropolitan University, Osaka 599-8531, Japan
7 Division of Applied Chemistry, Graduate School of Engineering, Osaka University, Osaka 565-0871, Japan
8 RIKEN SPring-8 Center, 1-1-1 Kouto, Sayo-gun, Sayo-cho 679-5148, Japan
9 Japan Synchrotron Radiation Research Institute (JASRI), 1-1-1 Kouto, Sayo-gun, Sayo-cho 679-5198, Japan
10 Physics Department, Aristotle University of Thessaloniki, 54124 Thessaloniki, Greece
11 Faculty of Engineering, Kyoto University of Advanced Science, Kameoka 621-8555, Japan
* Correspondence: k.prassides@omu.ac.jp
† These authors contributed equally to this work.
‡ Present address: Nano Carbon Device Research Center, National Institute of Advanced Industrial Science and Technology (AIST), Tsukuba 305-8565, Japan.

Abstract: The endohedral lithium fulleride, $Li^+@C_{60}^{\bullet-}$, is a potential precursor for new families of molecular superconducting and electronic materials beyond those accessible to date from C_{60} itself. Solid Li@C_{60} comprises $(Li@C_{60})_2$ dimers, isostructural and isoelectronic with the $(C_{59}N)_2$ units found in solid azafullerene. Here, we investigate the structural and vibrational properties of Li@C_{60} samples synthesized by electrolytic reduction routes. The resulting materials are of high quality, with crystallinity far superior to that of their antecedents isolated by chemical reduction. They permit facile, unambiguous identification of both the reduced state of the fulleride units and the interball C-C bonds responsible for dimerization. However, severe orientational disorder conceals any crystal symmetry lowering due to the presence of dimers. Diffraction reveals the adoption of a hexagonal crystal structure (space group $P6_3/mmc$) at both low temperatures and high pressures, typically associated with close-packing of spherical monomer units. Such a situation is reminiscent of the structural behavior of the high-pressure Phase I of solid dihydrogen, H_2.

Keywords: endofullerenes; dimerization; vibrational spectroscopy; synchrotron X-ray diffraction; high pressure

Citation: Vrankić, M.; Nakagawa, T.; Menelaou, M.; Takabayashi, Y.; Yoshikane, N.; Matsui, K.; Kokubo, K.; Kato, K.; Kawaguchi-Imada, S.; Kadobayashi, H.; et al. On the Structural and Vibrational Properties of Solid Endohedral Metallofullerene Li@C_{60}. *Inorganics* **2024**, *12*, 99. https://doi.org/10.3390/inorganics12040099

Academic Editor: David Turner

Received: 3 March 2024
Revised: 28 March 2024
Accepted: 28 March 2024
Published: 29 March 2024

1. Introduction

Following the serendipitous discovery of the fullerene family of molecular carbon nearly 40 years ago, research on the chemical, physical, and materials properties of its members and those of their derivatives has proceeded unabated. In brief, there are four distinct ways of manipulating the molecular and crystalline forms of the fullerenes. Firstly, direct chemical functionalization of the π-electron molecular framework leads to a rich organic chemistry, affording numerous derivatives of both C_{60} and its higher fullerene antecedents that have applications in diverse fields from molecular electronics to solar cells [1].

Secondly, reductive intercalation of metal ions into the voids of the crystalline structures of fullerenes—most prominently, that of C_{60}—leads to sensitively modifying the electronic structure and has resulted in a plethora of fulleride salts with M_xC_{60} stoichiometry and x ranging from a low value of 1 (e.g., in RbC_{60}) to a high value of 12 (e.g., in $Li_{12}C_{60}$). In particular, exohedrally modified fulleride materials with A_3C_{60} (A = alkali metal) stoichiometry have provided examples of high-T_c molecular superconductors with transition temperatures as high as 38 K and with the zero-resistance performance surviving to record high magnetic fields (exceeding 90 T). Of significance is also the unconventional, highly correlated nature of superconductivity, which is proximate to an antiferromagnetic Mott insulating state out of which it emerges upon lattice contraction via the application of chemical and/or physical pressure [2–5].

Thirdly, the electronic structure can be tuned by on-ball substitution of heteroatoms such as B or N. The most prominent derivative has been the azafullerene radical, $C_{59}N^{\bullet}$, which dimerizes to afford the non-magnetic $(C_{59}N)_2$ moiety [6]. Further manipulation of the properties of such heterofullerenes can be achieved by exohedral metal intercalation, resulting in salts such as $K_6C_{59}N$, in which electron doping is achieved synergistically both by on- and in-between-the-balls donors [7].

Finally, a large family of fullerene derivatives can be accessed by endohedral encapsulation of atomic or molecular units to afford $A@C_n$ moieties. For a long while, this field of fullerene research was dominated by metal encapsulation of higher fullerenes [8,9], with bulk availability of endohedral C_{60} units remaining elusive. This situation has changed dramatically following two significant discoveries: (a) the development of the "molecular surgery" synthetic technique [10], which has led to numerous endohedral C_{60} fullerenes incorporating noble gas atoms (e.g., He, Ne, Ar, Kr) or small molecules (e.g., H_2, HF, CO, H_2O, CH_4) [11,12] and (b) the successful synthesis of fullerene salts, $(Li^+@C_{60})X^-$ ($X^- = PF_6^-$, $SbCl_6^-$), which comprise $Li^+@C_{60}$ endohedral molecular ions and X^- spacer units, which serve a charge-balancing role [13–15]. Remarkably, both chemical and electrochemical reduction of the $Li^+@C_{60}$ cation lead to the formation of the neutral radical anion, $Li^+@C_{60}^{\bullet-}$ [16,17], which, in analogy with the on-ball-substituted azafullerene $C_{59}N^{\bullet}$ radical, dimerizes to afford $(Li@C_{60})_2$, isostructural and isoelectronic with the $(C_{59}N)_2$ molecule [18,19].

Structural and electronic characterization of the $(Li@C_{60})_2$ solid obtained by chemical reduction confirmed its dimeric structure in the solid state [17]. However, the as-obtained material lacked good crystallinity, resulting in moderate quality diffraction and spectroscopic data. Attempts to sublime the material led to the escape of the metal ion from the endofullerene space, precluding any improvement in crystallinity, in contrast to its azafullerene antecedent [19]. Here, we report on the structural and vibrational properties of the $(Li@C_{60})_2$ solid obtained by electrochemical reduction—this is a highly crystalline material, which permits detailed study of the structural and electronic properties. While vibrational spectroscopy readily identifies the vibrational signatures of interball C-C bond formation consistent with dimerization, the material is shown to adopt a highly symmetric hexagonal-close-packed crystal structure—typically associated with monomer sphere packing—as a result of disorder both at ambient pressure down to 3.4 K and at ambient temperature up to 13.1 GPa.

2. Results and Discussion

2.1. Vibrational Properties

The Raman spectrum of $(Li@C_{60})_2$ obtained by electrochemical reduction of the $(Li^+@C_{60})(PF_6^-)$ precursor, along with those of monomeric C_{60}, $(Li@C_{60})(PF_6)$, and dimeric $(C_{59}N)_2$ solids, is illustrated in Figure 1—the corresponding molecular units are generated by VESTA [20]. The frequencies of the observed Raman peaks are summarized in Table S1. In the case of the monomeric C_{60} and $(Li@C_{60})(PF_6)$ fullerene materials, the 785 nm laser line was used for excitation to prevent photoinduced polymerization upon illumination with visible or ultraviolet light [21]. On the other hand, owing to the stability of the dimeric

$(Li@C_{60})_2$ and $(C_{59}N)_2$ fullerenes against photoinduced polymerization, the 633 nm line of a He-Ne laser was used for their excitation to take advantage of the improved throughput of the Raman spectrometer in the corresponding spectral region. The Raman spectra of C_{60} solid and $(Li@C_{60})(PF_6)$ are nearly identical to each other with small frequency shifts ($\leq$3 cm^{-1}) between the corresponding peaks and are compatible with the monomeric nature of the C_{60} units. Both spectra are dominated by the ten Raman-active intramolecular C_{60} modes, attributed to the two totally symmetric $A_g(1)$ and $A_g(2)$ modes and the eight fivefold-degenerate $H_g(1)$-$H_g(8)$ of the C_{60} molecule in icosahedral I_h symmetry [22]. The weak crystal field in solid C_{60} causes only the splitting of the radial $H_g(1)$ mode into two components (at 266 and 272 cm^{-1}), while the appearance of a weak peak at 1458 cm^{-1} can be attributed to the presence of traces of polymerized C_{60} ($A_g(2)$ mode of polymeric chains [23]).

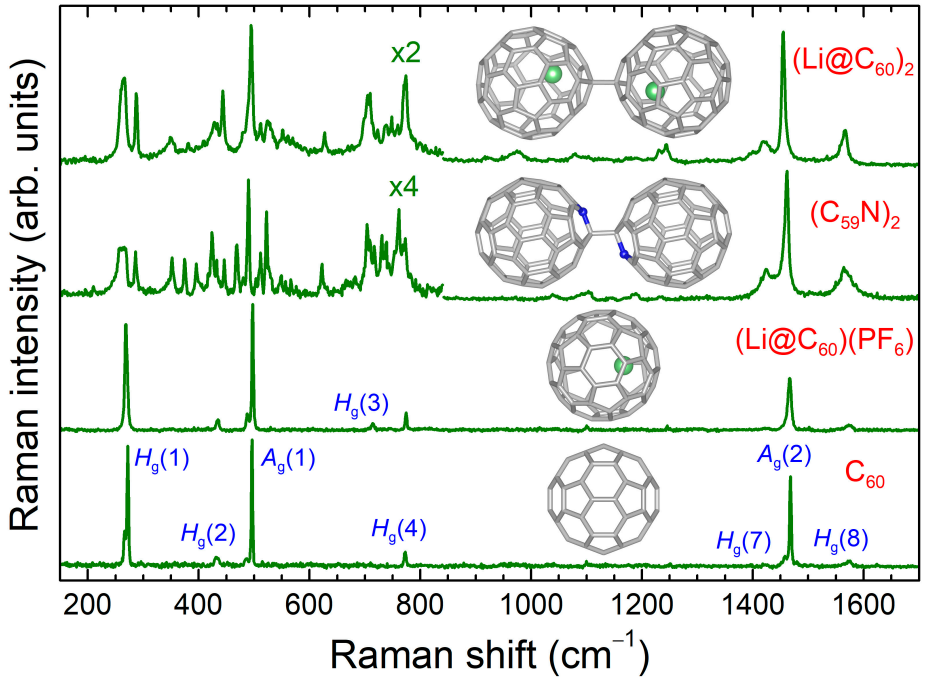

Figure 1. The Raman spectrum of the $(Li@C_{60})_2$ sample prepared by electrochemical reduction (λ_{exc} = 633 nm) is displayed together with those of C_{60} (λ_{exc} = 785 nm), monomeric $(Li@C_{60})(PF_6)$ (λ_{exc} = 785 nm), and dimeric $(C_{59}N)_2$ (λ_{exc} = 633 nm) solids. The low-frequency spectral region in the dimeric molecular solids has been suitably enhanced to improve visibility. The mode assignment refers to the irreducible representations of the C_{60} molecule in I_h symmetry. Each spectrum is accompanied by the structure of the corresponding molecular unit drawn by VESTA [20].

The Raman spectrum of dimeric $(C_{59}N)_2$ solid is far richer in structure compared to the monomeric systems, as the cage distortion and the concomitant lowering of the molecular symmetry upon dimerization cause the appearance of additional Raman peaks. These originate from the splitting of the degenerate H_g modes and the activation and splitting of inactive vibrational modes of the C_{60} molecule in I_h symmetry [24,25]. The plethora of Raman split components appearing in the spectrum of $(C_{59}N)_2$ is in fair agreement with those earlier reported in the literature and assigned to intramolecular C_{60} modes in I_h symmetry [24]. The same assignment of the observed Raman peaks in the present work was also adopted in Table S1. As inferred from Figure 1 and Table S1, the similarity of the Raman spectrum profile and the frequencies of the constituent Raman peaks of $(Li@C_{60})_2$ obtained by electrochemical reduction with those of dimeric $(C_{59}N)_2$ is evident, establishing its dimeric nature unambiguously. Moreover, comparison of the overall Raman spectrum profile of the present $(Li@C_{60})_2$ sample with that of the neutral $Li@C_{60}$ obtained by chemical reduction of the $Li^+@C_{60}$ cation by decamethylferrocene (Figure S1) clearly illustrates the

stronger intensities and narrower lineshapes of the split Raman components in $(Li@C_{60})_2$ obtained by electrochemical reduction—this is in addition to the similarities regarding the appearance of the Raman peaks associated with the dimerization of the C_{60} cages. The present results are compatible with the superior crystallinity of the present material, in accordance with its powder XRD data (*vide infra*), contrary to the situation encountered in $(Li@C_{60})_2$ obtained by chemical reduction, where a small fraction of monomers is also present [17].

The frequency of the $A_g(2)$ pentagonal pinch mode of the C_{60} molecule deserves further attention. In particular, the $A_g(2)$ frequency in C_{60}-based materials is extremely sensitive to both doping and intermolecular covalent bonding [23–28]. In monomeric alkali fullerides, it downshifts quasi-linearly by 6–7 cm^{-1} per electron transferred from the metal atoms to the C_{60} units [26–28], due to the elongation of the intramolecular bonds induced by the charge transfer process and the resulting softening of the force constants [29,30]. Moreover, in neutral polymeric C_{60}-based fullerene materials—including dimerized systems—the $A_g(2)$ mode also softens due to the intermolecular covalent bond formation and the concomitant decrease in the mean intramolecular bond strength. The observed softening depends strongly on the number of the sp^3-like coordinated carbon atoms per molecular cage [31]. Accordingly, and as evident in Table S1 (numbers in bold), there is a softening of the $A_g(2)$ peak in neutral $(C_{59}N)_2$ compared to that in C_{60} solid by ~6 cm^{-1}, which is attributed to the formation of the intermolecular covalent bond due to dimerization [25]. In the case of $(Li@C_{60})_2$, the softening of this peak is even larger, ~13 and ~10 cm^{-1} relative to monomeric C_{60} and $(Li@C_{60})(PF_6)$, respectively. This can be understood in terms of the combined effect of covalent intermolecular bonding and uptake of one electron by the C_{60} cage in $(Li@C_{60})_2$—here, electrons are more delocalized over the radical carbanion cage than in the case of $(C_{59}N)_2$, where the electron pairs are localized on the nitrogen atoms [17].

The dimeric nature of $(Li@C_{60})_2$ obtained by electrochemical reduction is further supported by its IR transmission spectrum illustrated in Figure 2 in comparison with that of monomeric C_{60} solid. More specifically, the IR spectrum of C_{60} solid is dominated by the four IR active modes of the C_{60} molecule in I_h symmetry $\{F_{1u}(1)$-$F_{1u}(4)\}$, appearing at 525, 576, 1182, and 1428 cm^{-1}, in excellent agreement with the literature [32]. The additional weaker spectral features are due to forbidden fundamentals, activated by the distortion of the molecular I_h symmetry in the C_{60} crystal. As in the case of the corresponding Raman spectrum, in the IR spectrum of $(Li@C_{60})_2$, several split components appear due to intercage bonding and symmetry lowering, similar to the case of $(C_{59}N)_2$ [33]. Despite similarities of the IR spectrum with that of monomeric $C_{59}HN$, the appearance of characteristic features in the frequency region 800–850 cm^{-1} (marked accordingly in Figure 2) provides a fingerprint of the dimerization of the molecular cages [33].

2.2. Structural Properties at Ambient Pressure

The synchrotron X-ray powder diffraction patterns of the $(Li@C_{60})_2$ sample recorded at 300 and 3.4 K at ambient pressure are shown in Figure 3. An immediate observation is that they appear strikingly similar to those reported for as-prepared solid $(C_{59}N)_2$, in terms of both the position and the relative intensity of the diffraction peaks present [18,34]. As-prepared $(C_{59}N)_2$ crystallizes in a hexagonal lattice (space group $P6_3/mmc$) with lattice constants at ambient temperature, a = 9.97 Å and c = 16.18 Å [18]. In a remarkable analogy, the patterns of $(Li@C_{60})_2$ prepared by electrochemical reduction are also consistent with the material adopting an isostructural hexagonal closed-packed (*hcp*) arrangement of the fullerene units with a somewhat smaller (c/a) anisotropy (space group $P6_3/mmc$, at 300 K: a = 10.04374(10) Å and c = 16.13451(19) Å; at 3.4 K: a = 9.9560(3) Å and c = 16.0317(5) Å). Excellent refinements of the diffraction profiles are achieved by the LeBail pattern–decomposition technique using the GSAS suite (at 300 K: R_{wp} = 1.88%, R_{exp} = 1.48%; at 3.4 K: R_{wp} = 2.23%, R_{exp} = 1.43%) (Figure 3).

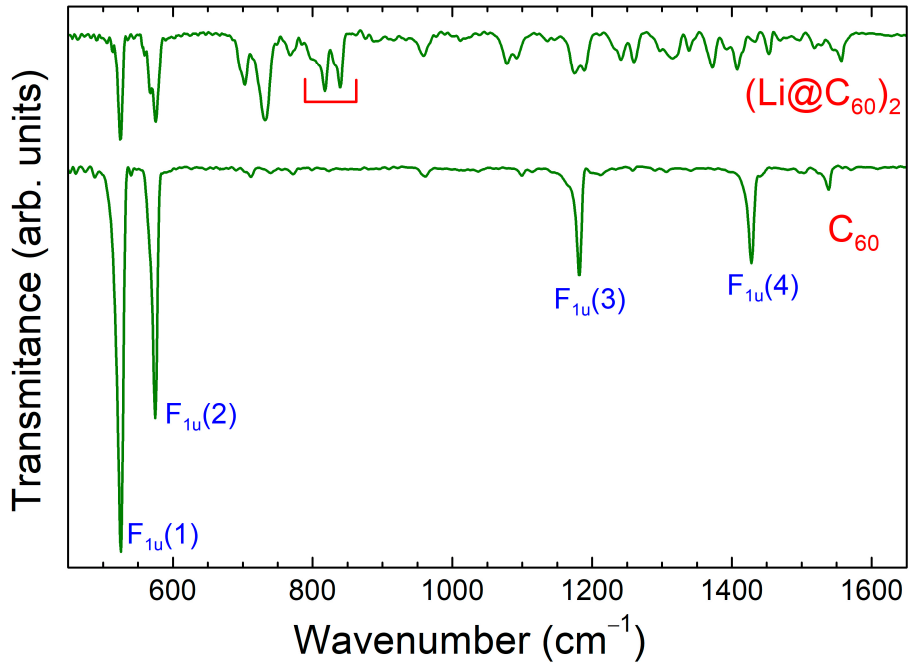

Figure 2. IR transmission spectrum of the $(Li@C_{60})_2$ sample prepared by electrochemical reduction and compared to that of solid C_{60}. Characteristic "dimer peaks" in the frequency region 800–850 cm^{-1} are indicated. The mode assignment refers to the irreducible representations of the C_{60} molecule in I_h symmetry.

On the other hand, the measured profiles of the present $(Li@C_{60})_2$ sample contrast sharply with those of both $(Li@C_{60})_2$ prepared by chemical reduction route [17] and sublimed $(C_{59}N)_2$ [19]. The former displays a powder pattern, which can be indexed on a pseudo-cubic unit cell with a lattice size of ~14.15 Å (interfullerene separation ~10.01 Å) [17], whereas the latter provides clear evidence of a dimerized molecular structure and a lowering of crystal symmetry to monoclinic [19].

The apparent *hcp* crystal structure (Figure 3a inset) of $(Li@C_{60})_2$ prepared by electrochemical reduction is an archetypal packing arrangement of monomer units. Therefore, it is counterintuitive and contrasts sharply with the dimerization of the molecular units that has been unambiguously established by vibrational spectroscopy (*vide supra*). In the $P6_3/mmc$ space group, the $Li@C_{60}$ balls reside in the 2*d* positions, (⅔, ⅓, ¼) and (⅓, ⅔, ¾). As a result, their center-to-center distance at ambient temperature is 9.94 Å, implicit of the absence of interball bond formation. Due to the translational symmetry of the hexagonal unit cell, there are six nearest neighbors at this distance of 9.94 Å, together with six additional ones in the *ab* pane at 10.04 Å. These are close to the C_{60}—C_{60} distances in monomeric C_{60} (~10 Å) and are longer than those (~9.34 Å) in typical dimerized C_{60} structures like that of RbC_{60} [35–37].

The inconsistency with the vibrational results may be resolved if we introduce orientational disorder of the dimer units residing on the *hcp* sites. To this effect, we recall a much-celebrated analogous situation—namely, that of the Phase I of solid dihydrogen, H_2 [38]. At room temperature, this phase is stable between 5 and 190 GPa and comprises freely rotating dihydrogen molecules, forming an *hcp* crystal structure (space group $P6_3/mmc$). We therefore attempted Rietveld refinements of the diffraction data by modeling the pronounced orientational disorder of the fullerene moieties in terms of spherical shell scatterers placed at the 2*d* sites of $\bar{6}m2$ symmetry in the *hcp* lattice. In the course of the refinements, we found it necessary to also introduce scattering density at the 2*a* sites of $\bar{3}m$. symmetry, presumably reflecting the presence of residual CH_2Cl_2 solvent molecules intercalated during the electrochemical synthetic protocol. Rietveld refinements now proceeded smoothly, resulting in a stoichiometry of $(Li@C_{60})_2 \cdot (CH_2Cl_2)_{0.81(2)}$ for the material. We note

that an analogous situation was encountered in the Rietveld refinements of the diffraction data of as-prepared *hcp*-structured azafullerene solid, whose stoichiometry was established as $(C_{59}N)_2 \cdot (CS_2)_{1.0}$ [34]. The refinement results are shown in Figure 4 and Table S2.

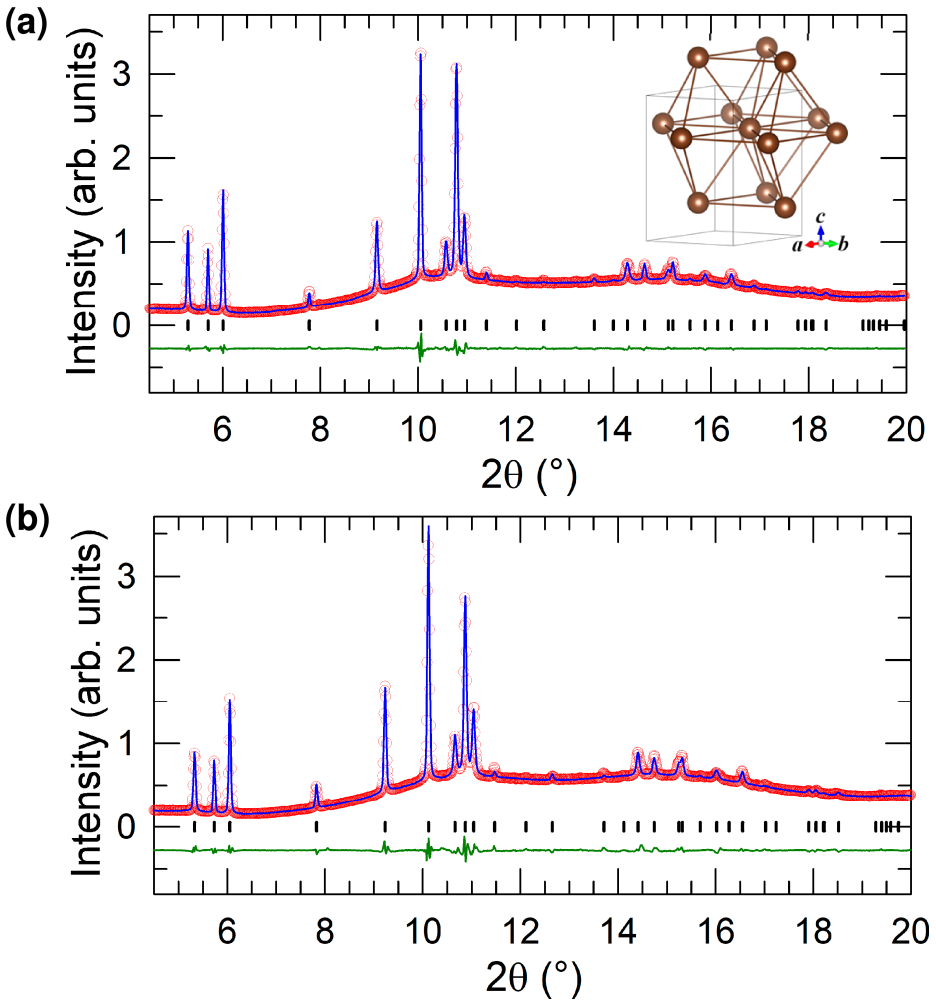

Figure 3. LeBail refinements (using the GSAS suite of programs) of the synchrotron X-ray (λ = 0.80031 Å) powder diffraction profiles of $(Li@C_{60})_2$ at (**a**) 300 K and (**b**) 3.4 K. The red open circles represent the measured intensity, and the blue solid line shows the calculated intensity. The lower green solid line shows the difference profile, and the tick marks show the reflection positions in space group $P6_3/mmc$. The inset in (**a**) shows a schematic diagram of the apparent hexagonal close-packing motif of solid spheres, consistent with the space group symmetry.

Figure 5a,b shows the temperature dependence of the unit–cell volume and the lattice parameters *a* and *c*, as extracted from the LeBail analyses of the diffraction data. The smooth evolution in lattice size confirms the absence of any structural phase transition down to 3.4 K. The only apparent effect is a decrease in the lattice anisotropy, as measured by the (c/a) ratio, which monotonically increases with decreasing temperature, approaching a value just larger than 1.61 at 3.4 K (Figure 5c). This is still smaller than the ideal value of 1.633 in perfect hexagonal close-packed architectures, but the decreased anisotropy on cooling may reflect a partial freezing out of the orientational disorder of the fullerene units.

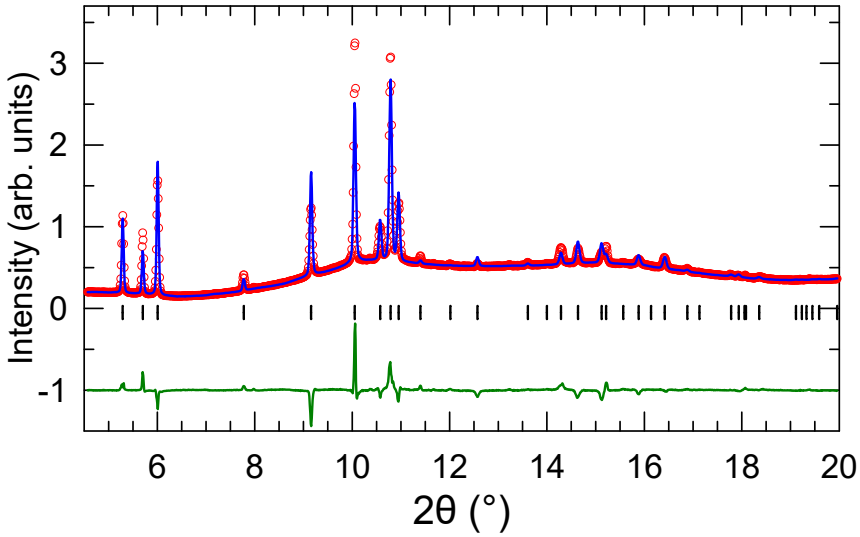

Figure 4. Rietveld analysis result (space group $P6_3/mmc$) using the Fullprof suite of programs—final observed (red circles) and calculated (blue solid line) synchrotron X-ray (λ = 0.80031 Å) powder diffraction profiles for the $(Li@C_{60})_2$ sample at 300 K. The lower solid line shows the difference profile, and the tick marks show the reflection positions. Refined parameters and agreement indices are provided in Supplementary Information, Table S2.

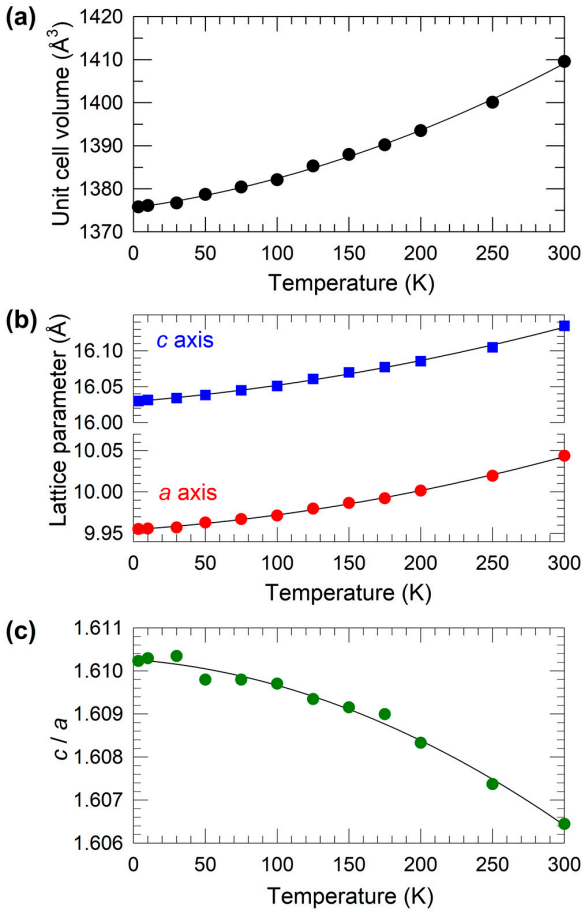

Figure 5. Temperature dependence of (**a**) the unit cell volume, (**b**) the hexagonal lattice constants, *a* and *c*, and (**c**) the (*c*/*a*) ratio in $(Li@C_{60})_2$ at ambient pressure. The lines through the points are guides-to-the-eye.

2.3. Structural Properties at High Pressure

Synchrotron X-ray powder diffraction data of $(Li@C_{60})_2$ were collected at ambient temperature and at selected pressures between 0.5 and 13.1 GPa. As the pressure increases, the diffraction profiles show gradual Bragg peak shifting towards higher 2θ angles consistent with unit cell contraction; this is accompanied by some peak broadening due to increasing inhomogeneities upon pressurization (Figure 6). No evidence of the occurrence of any structural phase transition is found in the pressure range of the present experiments. All diffraction patterns index with the same hexagonal unit cell (space group $P6_3/mmc$) found at all temperatures at ambient pressure. Representative LeBail refinements at base and highest pressures are included in Figure 6 (at 0.5 GPa: a = 9.89824(18) Å and c = 15.9333(3) Å; R_{wp} = 0.35%, R_{exp} = 4.60%; at 13.1 GPa: a = 9.2495(5) Å and c = 15.0437(11) Å; R_{wp} = 0.29%, R_{exp} = 4.94%). The evolution of the $(Li@C_{60})_2$ unit cell dimensions upon pressurization was investigated by LeBail refinements of the diffraction profiles (Figure 7a,b). Some spurious weak peaks, which were present in the diffraction datasets when the sample was introduced into the diamond anvil cell (DAC)—but were absent for the same sample batch outside the pressure cell—were excluded from the refinements. Figure 7c displays the change in the lattice anisotropy of the *hcp* structure, as monitored by the evolution of the (c/a) ratio. Upon pressurization, c/a increases monotonically at the beginning but eventually saturates above ~10 GPa towards a value of ~1.626, close to the ideal value of 1.633 expected for perfect *hcp* stacking of solid spheres. Comparable behavior was also observed before for the isostructural dimeric $(C_{59}N)_2$ solid, in which the (c/a) ratio approached ~1.633 at ~6.5 GPa [18]. Such behavior implies that, at these elevated pressures, the intradimer and interdimer C-C distances in the compressed material have become comparable. Notably, this occurs in the same pressure range that the interdimer center-to-center separations in $(Li@C_{60})_2$ have decreased to values on the order of ~9.2–9.3 Å. Such close interball contacts have provided the signature of single C-C bond formation in fullerene-derived polymers [35–37] before.

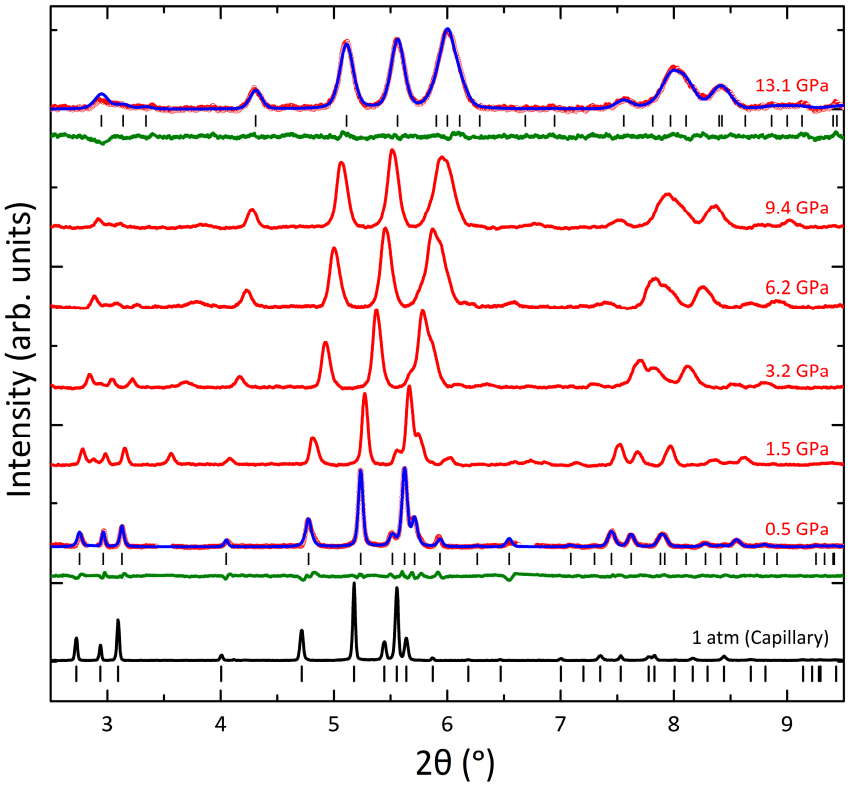

Figure 6. Representative high-pressure synchrotron X-ray powder diffraction profiles after background subtraction (λ = 0.4128 Å) of $(Li@C_{60})_2$ (red solid lines and open circles) at elevated pressures.

The corresponding diffraction profile at 1 atm (capillary) from Figure 5 is also displayed for comparison after conversion to the same wavelength (black solid line). The LeBail refinement results for base (0.5 GPa) and highest (13.1 GPa) pressure are also included (blue solid lines: calculated, red circles: observed). Tick marks label the reflections of the hexagonal lattice (space group $P6_3/mmc$), and the green solid lines are the difference profiles between observed and calculated profiles. Some spurious weak peaks present in the high-pressure data with the sample inside the diamond anvil cell (DAC) are excluded from the refinements.

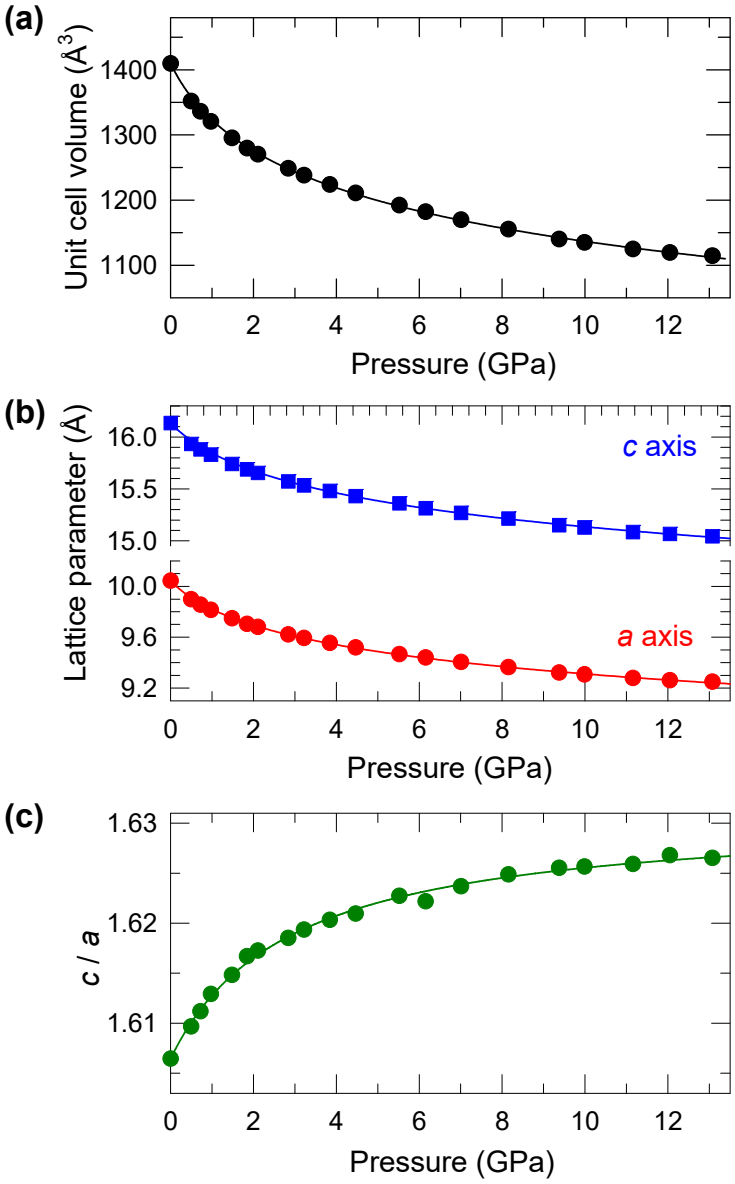

Figure 7. Pressure dependence of (**a**) the unit cell volume, (**b**) the hexagonal lattice constants, a and c, and (**c**) the (c/a) ratio in $(Li@C_{60})_2$ at ambient temperature. The solid lines in (**a**,**b**) are the results of least-squares fits to the semi-empirical 2nd-order Murnaghan equation-of-states (EoS) and its axial compressibility variants, respectively. The line through the points in (**c**) is a guide-to-the-eye.

The pressure dependence of the unit cell volume of $(Li@C_{60})_2$ was next investigated using the semi-empirical second-order Murnaghan equation-of-state (EoS):

$$P = \left(\frac{K_0}{K_0{}'}\right)\left[\left(\frac{V_0}{V}\right)^{K_0{}'} - 1\right] \quad (1)$$

where K_0 is the atmospheric pressure isothermal bulk modulus, K_0' is its pressure derivative ($\equiv dK_0/dP)_{P=0}$, and V_0 is the unit–cell volume at zero pressure (approximated by the ambient pressure datum at 1 atm; here, V_0 = 1409.58 Å^3). The EoS fit to the $V(P)$ data (see Equation (S1) in the Supplementary Materials) of $(Li@C_{60})_2$ up to a pressure of 13.1 GPa results in values of K_0 = 10.8(3) GPa (leading to an initial volume compressibility, $\kappa = -d\ln V/dP$ = 0.093(3) GPa^{-1}) and of K_0' = 11.4(2) (Figure 7a). The measured volume compressibility of $(Li@C_{60})_2$ is higher than those of $(C_{59}N)_2$ (κ = 0.046(2) GPa^{-1}) and of the monomeric C_{60} (κ = 0.055 GPa^{-1}) and $(Li^+@C_{60})(PF_6)$ (κ = 0.0571(4) GPa^{-1}) [15,18,39] solids, implying more flexible nearest-neighbor bonds and somewhat less tight crystal packing. Modified EoS equations, in which K_0 and its pressure derivative, K_0', were replaced by K_x and K_x' ($x = a$ or c) parameters, were used to fit the corresponding lattice axes data to extract initial axial compressibilities, β_x (= $1/(3K_x)$ GPa^{-1}, $x = a$ or c) (Figure 7b). As anticipated by the earlier discussion on the pressure dependence of the (c/a) ratio, we find that the compressibility along the c-axis (β_c = 0.0086(2) GPa^{-1}) is smaller than that along the a-axis (β_a = 0.0112(3) GPa^{-1}). Such a pressure response was also observed for $(C_{59}N)_2$ and was then interpreted as a consequence of the intradimer bonds being oriented along the (1/3, 2/3, 1/2) direction and therefore inclined at a larger angle to the basal plane than to the c-axis [18].

3. Materials and Methods

The $(Li^+@C_{60})(PF_6^-)$ sample used as a precursor in the present work was purchased from Idea International Corporation. Its electrochemical reduction to afford $(Li@C_{60})_2$ was performed according to the experimental protocol described in the literature before [16].

Raman spectra of $(Li@C_{60})_2$ were recorded in backscattering geometry using a LabRam HR (HORIBA, Kyoto, Japan) micro-Raman spectrometer, equipped with a Peltier cooled CCD detector. Laser lines at 633 and 785 nm were alternatively used for excitation, focused on the samples by means of a 100× objective at a power lower than 0.3 mW to avoid any laser-heating-induced effects.

Infrared (IR) transmission spectra of the samples under argon atmosphere were collected by means of a JASCO (Tokyo, Japan) FT-IR 6200 spectrometer.

Synchrotron X-ray powder diffraction measurements of $(Li@C_{60})_2$ at various temperatures between 3.4 and 300 K at ambient pressure were performed with the high-resolution powder diffractometer on beamline BL44B2 at SPring-8, Hyogo, Japan using a helium-flow cryostat [40]. The powder sample was sealed in a 0.5 mm diameter thin-wall glass capillary under He gas. The wavelength was 0.800312(1) Å. LeBail and Rietveld analyses were performed with the GSAS and Fullprof suites of refinement programs [41–43].

Synchrotron X-ray powder diffraction measurements of $(Li@C_{60})_2$ up to 13.1 GPa at ambient temperature were conducted at the BL10XU beamline, SPring-8, Hyogo, Japan. The powder X-ray diffraction data (monochromatized beam with λ = 0.41277(5) Å, beam size = 40 μm) were collected on an image plate detector (Rigaku (Tokyo, Japan) R-AXIS IV^{++}, 300 × 300 mm^2, and 0.10 mm pixel size) while oscillating the sample [44]. Masking of the Bragg reflections of the DAC and integration of the 2D diffraction images to afford one-dimensional diffraction profiles were processed with the IPanalyzer software [45]. LeBail analysis of the diffraction profiles was performed with the GSAS suite of refinement programs [41,42]. A DAC [46,47], equipped with single-crystal diamonds of 500 μm culet diameter and with an 80 μm-thick stainless-steel gasket, was used for pressure generation. Powder samples were introduced into 250 μm diameter holes made at the center of the gasket, together with a ruby sphere and helium gas (solidification pressure ~12.1 GPa at room temperature, pressure uncertainty less than 0.5% at the highest pressure of the present experiment [48]) as pressure marker and pressure medium, respectively. The applied pressure was measured by the ruby–fluorescence method [49]. All measured pressure values are quoted to one decimal point.

4. Conclusions

In conclusion, we have presented a detailed structural and vibrational characterization of the dimerized endohedral metallofullerene, $(Li@C_{60})_2$, in the solid state. The material used in the present work was obtained by electrochemical reduction of the trifluoromethanesulfonyl imide precursor salt, $(Li^+@C_{60})(TFSI^-)$ [16]. Its highly crystalline nature permits facile identification of spectroscopic features related to interfullerene C-C bonding. Remarkably, the crystal structure of the material remains hexagonal close-packed (space group $P6_3/mmc$) both at low temperatures and ambient pressure and at high pressures and ambient temperature, concealing the effects of dimerization and the anticipated lowering in symmetry. High orientational disorder (together with the presence of some residual dichloromethane solvent) can account for the apparent high symmetry. A comparable orientational disorder scenario has been used to rationalize the *hcp* Phase I of solid dihydrogen (H_2) at high pressures.

Supplementary Materials: The following supporting information can be downloaded at: https://www.mdpi.com/article/10.3390/inorganics12040099/s1, Figure S1: Comparison of Raman spectra of $(Li@C_{60})_2$ obtained by chemical and electrochemical reduction; Table S1: Assignment of observed Raman peaks and their frequencies for C_{60}, $(Li@C_{60})(PF_6)$, $(C_{59}N)_2$, and $(Li@C_{60})_2$; Table S2: Refined parameters of the Rietveld analysis of the synchrotron X-ray powder diffraction data of $(Li@C_{60})_2$; Equation (S1): $V(P)$ form of the Murnaghan equation-of-state.

Author Contributions: Synthesis, M.V., T.N. and K.K. (Ken Kokubo); synchrotron X-ray diffraction—data collection and analysis, M.V., T.N., M.M., Y.T., K.K. (Kenichi Kato) and K.P.; high-pressure synchrotron X-ray diffraction—data collection and analysis, N.Y., K.M., S.K.-I., H.K. and K.P.; vibrational spectroscopy, J.A.; conceptualization and overall conclusions, J.A., Y.K. and K.P.; project supervision, K.P.; writing—review and editing, K.P. All authors have read and agreed to the published version of the manuscript.

Funding: This research was financially supported by Grants-in-Aid for Scientific Research (JSPS KAKENHI grant numbers JP18K05254, JP21H01907, JP22K18693, and JP23KJ1843) and by JST SPRING, grant number JPMJSP2139.

Data Availability Statement: All data supporting the reported results in this paper can be obtained from the authors.

Acknowledgments: We thank SPring-8 for access to synchrotron XRPD measurements (proposal no. 2017A4131, 2017A1363, 2017B1276, 2017B1358, 2018A1398, and 2022A1699).

Conflicts of Interest: The authors declare no conflicts of interest.

References

1. Hirsch, A.; Brettreich, M. *Fullerenes: Chemistry and Reactions*; Wiley-VCH, 5 Wiley-VCH Verlag GmbH & Co. KgaA: Weinheim, Germany, 2005.
2. Takabayashi, Y.; Prassides, K. Unconventional high-T_c superconductivity in fullerides. *Philos. Trans. R. Soc. A Math. Phys. Eng. Sci.* **2016**, *374*, 20150320. [CrossRef] [PubMed]
3. Zadik, R.H.; Takabayashi, Y.; Klupp, G.; Colman, R.H.; Ganin, A.Y.; Potocnik, A.; Jeglic, P.; Arcon, D.; Matus, P.; Kamaras, K.; et al. Optimized unconventional superconductivity in a molecular Jahn-Teller metal. *Sci. Adv.* **2015**, *1*, e1500059. [CrossRef]
4. Nomura, Y.; Sakai, S.; Capone, M.; Arita, R. Unified understanding of superconductivity and Mott transition in alkali-doped fullerides from first principles. *Sci. Adv.* **2015**, *1*, e1500568. [CrossRef] [PubMed]
5. Kasahara, Y.; Takeuchi, Y.; Zadik, R.H.; Takabayashi, Y.; Colman, R.H.; McDonald, R.D.; Rosseinsky, M.J.; Prassides, K.; Iwasa, Y. Upper critical field reaches 90 tesla near the Mott transition in fulleride superconductors. *Nat. Commun.* **2017**, *8*, 14467. [CrossRef] [PubMed]
6. Hummelen, J.C.; Knight, B.; Pavlovich, J.; Gonzalez, R.; Wudl, F. Isolation of the heterofullerene $C_{59}N$ as its dimer $(C_{59}N)_2$. *Science* **1995**, *269*, 1554–1556. [CrossRef] [PubMed]
7. Prassides, K.; Keshavarz-K, M.; Hummelen, J.C.; Andreoni, W.; Giannozzi, P.; Beer, E.; Bellavia, C.; Cristofolini, L.; Gonzalez, R.; Lappas, A.; et al. Isolation, structure, and electronic calculations of the heterofullerene salt $K_6C_{59}N$. *Science* **1996**, *271*, 1833–1835. [CrossRef]
8. Shinohara, H.; Tagmatarchis, N. *Endohedral Metallofullerenes: Fullereness with Metal Inside*; Wiley: Chichester, UK, 2015.
9. Akasaka, T.; Nagase, S. *Endofullerenes: A New Family of Carbon Clusters*; Springer: Dordrecht, The Netherlands, 2002.

10. Komatsu, K.; Murata, M.; Murata, Y. Encapsulation of molecular hydrogen in fullerene C_{60} by organic synthesis. *Science* **2005**, *307*, 238–240. [CrossRef] [PubMed]
11. Bloodworth, S.; Whitby, R.J. Synthesis of endohedral fullerenes by molecular surgery. *Commun. Chem.* **2022**, *5*, 121. [CrossRef] [PubMed]
12. Krachmalnicoff, A.; Bounds, R.; Mamone, S.; Alom, S.; Concistrè, M.; Meier, B.; Kouřil, K.; Light, M.E.; Johnson, M.R.; Rols, S.; et al. The dipolar endofullerene HF@C_{60}. *Nat. Chem.* **2016**, *8*, 953–957. [CrossRef]
13. Aoyagi, S.; Nishibori, E.; Sawa, H.; Sugimoto, K.; Takata, M.; Miyata, Y.; Kitaura, R.; Shinohara, H.; Okada, H.; Sakai, T.; et al. A layered ionic crystal of polar $Li^+@C_{60}$ superatoms. *Nat. Chem.* **2010**, *2*, 678–683. [CrossRef]
14. Aoyagi, S.; Sado, Y.; Nishibori, E.; Sawa, H.; Okada, H.; Tobita, H.; Kasama, Y.; Kitaura, R.; Shinohara, H. Rock-salt-type crystal of thermally contracted C_{60} with encapsulated lithium cation. *Angew. Chem.* **2012**, *124*, 3433–3437. [CrossRef]
15. Colman, R.H.; Okur, H.E.; Garbarino, G.; Ohishi, Y.; Aoyagi, S.; Shinohara, H.; Prassides, K. Pressure effects on the crystal structure of the cubic metallofullerene salt [Li@C_{60}][PF_6] to 12 GPa. *Mater. Today Commun.* **2022**, *31*, 103275. [CrossRef]
16. Ueno, H.; Aoyagi, S.; Yamazaki, Y.; Ohkubo, K.; Ikuma, N.; Okada, H.; Kato, T.; Matsuo, Y.; Fukuzumi, S.; Kokubo, K. Electrochemical Reduction of Cationic $Li^+@C_{60}$ to Neutral $Li^+@C_{60}^{\cdot-}$: Isolation and Characterisation of Endohedral [60] Fulleride. *Chem. Sci.* **2016**, *7*, 5770–5774. [CrossRef] [PubMed]
17. Okada, H.; Ueno, H.; Takabayashi, Y.; Nakagawa, T.; Vrankic, M.; Arvanitidis, J.; Kusamoto, T.; Prassides, K.; Matsuo, Y. Chemical reduction of $Li^+@C_{60}$ by decamethylferrocene to produce neutral $Li^+@C_{60}^{\bullet-}$. *Carbon* **2019**, *153*, 467–471. [CrossRef]
18. Brown, C.M.; Beer, E.; Bellavia, C.; Cristofolini, L.; González, R.; Hanfland, M.; Häusermann, D.; Keshavarz-K, M.; Kordatos, K.; Prassides, K.; et al. Effects of Pressure on the Azafullerene $(C_{59}N)_2$ Molecular Solid to 22 GPa. *J. Am. Chem. Soc.* **1996**, *118*, 8715–8716. [CrossRef]
19. Brown, C.M.; Cristofolini, L.; Kordatos, K.; Prassides, K.; Bellavia, C.; González, R.; Keshavarz-K, M.; Wudl, F.; Cheetham, A.K.; Zhang, J.P.; et al. On the Crystal Structure of Azafullerene $(C_{59}N)_2$. *Chem. Mater.* **1996**, *8*, 2548–2550. [CrossRef]
20. Momma, K.; Izumi, F. VESTA 3 for three-dimensional visualization of crystal, volumetric and morphology data. *J. Appl. Crystallogr.* **2011**, *44*, 1272–1276. [CrossRef]
21. Rao, A.M.; Zhou, P.; Wang, K.-A.; Hager, G.T.; Holden, J.M.; Wang, Y.; Lee, W.-T.; Bi, X.-X.; Ecklund, P.C.; Cornett, D.S.; et al. Photoinduced polymerization of solid C_{60} films. *Science* **1993**, *259*, 955–957. [CrossRef]
22. Bethune, D.S.; Meijer, G.; Tang, W.C.; Rosen, H.J.; Golden, W.G.; Seki, H.; Brown, C.A.; de Vries, M.S. Vibrational Raman and infrared spectra of chromatographically separated C_{60} and C_{70} fullerene clusters. *Chem. Phys. Lett.* **1991**, *179*, 181–186. [CrossRef]
23. Davydov, V.A.; Kashevarova, L.S.; Rakhmanina, A.V.; Senyavin, V.M.; Ceolin, R.; Szwarc, H.; Allouchi, H.; Agafonov, V. Spectroscopic study of pressure-polymerized phases of C_{60}. *Phys. Rev. B* **2000**, *61*, 11936–11945. [CrossRef]
24. Kuzmany, H.; Plank, W.; Winter, J.; Dubay, O.; Tagmatarchis, N.; Prassides, K. Raman spectrum and stability of $(C_{59}N)_2$. *Phys. Rev. B* **1999**, *60*, 1005–1012. [CrossRef]
25. Plank, W.; Pichler, T.; Kuzmany, H.; Dubay, O.; Tagmatarchis, N.; Prassides, K. Resonance Raman excitation and electronic structure of the single bonded dimers $(C_{60}^{-})_2$ and $(C_{59}N)_2$. *Eur. Phys. J. B* **2000**, *17*, 33–42. [CrossRef]
26. Winter, J.; Kuzmany, H. Potassium doped fullerene K_xC_{60} with x = 0, 1, 2, 3, 4 and 6. *Solid State Commun.* **1992**, *84*, 935–938. [CrossRef]
27. Kuzmany, H.; Matus, M.; Burger, B.; Winter, J. Raman scattering in C_{60} fullerenes and fullerides. *Adv. Mater.* **1994**, *6*, 731–745. [CrossRef]
28. Kosaka, M.; Tanigaki, K.; Prassides, K.; Margadonna, S.; Lappas, A.; Brown, C.M.; Fitch, A.N. Superconductivity in Li_xCsC_{60} fullerides. *Phys. Rev. B* **1999**, *59*, R6628–R6630. [CrossRef]
29. Jishi, R.A.; Dresselhaus, M.S. Mode softening and mode stiffening in C_{60} doped with alkali metals. *Phys. Rev. B* **1992**, *45*, 6914–6918. [CrossRef] [PubMed]
30. Zhou, P.; Wang, K.A.; Wang, Y.; Eklund, P.C.; Dresselhaus, M.S.; Dresselhaus, G.; Jishi, R.A. Raman scattering in C_{60} and alkali-metal-saturated C_{60}. *Phys. Rev. B* **1992**, *46*, 2595–2605. [CrossRef] [PubMed]
31. Meletov, K.P.; Velkos, G.; Arvanitidis, J.; Christofilos, D.; Kourouklis, G.A. Raman study of the photopolymer formation in the {Pt(dbdtc)$_2$}·C_{60} fullerene complex and the decomposition kinetics of the photo-oligomers. *Chem. Phys. Lett.* **2017**, *68*, 124–129. [CrossRef]
32. Krause, M.; Dunsch, L.; Seifert, G.; Fowler, P.W.; Gromov, A.; Kratschmer, W.; Gutierrez, R.; Porezag, D.; Frauenheim, T.J. Vibrational signatures of fullerene oxides. *J. Chem. Soc. Faraday Trans.* **1998**, *94*, 2287–2294. [CrossRef]
33. Krause, M.; Baes-Fischlmair, S.; Pfeiffer, R.; Plank, W.; Pichler, T.; Kuzmany, H.; Tagmatarchis, N.; Prassides, K. Thermal Stability and high temperature graphitization of bisazafullerene $(C_{59}N)_2$ as studied by IR and Raman spectroscopy. *J. Phys. Chem. B* **2001**, *105*, 11964–11969. [CrossRef]
34. Prassides, K.; Wudl, F.; Andreoni, W. Solid Azafullerenes and Azafullerides. *Fullerene Sci. Technol.* **1997**, *5*, 801–812. [CrossRef]
35. Oszlányi, G.; Bortel, G.; Faigel, G.; Gránásy, L.; Bendele, G.M.; Stephens, P.W.; Forró, L. Single C-C Bond in $(C_{60})_2^{2-}$. *Phys. Rev. B* **1996**, *54*, 11849–11852. [CrossRef]
36. Prassides, K.; Vavekis, K.; Kordatos, K.; Tanigaki, K.; Bendele, G.M.; Stephens, P.W. Loss of cubic symmetry in low-temperature Na_2RbC_{60}. *J. Am. Chem. Soc.* **1997**, *119*, 834–835. [CrossRef]
37. Bendele, G.M.; Stephens, P.W.; Prassides, K.; Vavekis, K.; Kordatos, K.; Tanigaki, K. Effect of charge state on polymeric bonding geometry: The ground state of Na_2RbC_{60}. *Phys. Rev. Lett.* **1998**, *80*, 736–739. [CrossRef]

38. Ji, C.; Li, B.; Liu, W.; Smith, J.S.; Majumdar, A.; Luo, W.; Ahuja, R.; Shu, J.; Wang, J.; Sinogeikin, S.; et al. Ultrahigh-pressure isostructural electronic transitions in hydrogen. *Nature* **2019**, *573*, 558–562. [CrossRef]
39. Duclos, S.J.; Brister, K.; Haddon, R.C.; Kortan, A.R.; Thiel, F.A. Effects of Pressure and Stress on C_{60} Fullerite to 20 GPa. *Nature* **1991**, *351*, 380–382. [CrossRef]
40. Kato, K.; Tanaka, H. Visualizing charge densities and electrostatic potentials in materials by synchrotron X-ray powder diffraction. *Adv. Phys. X* **2016**, *1*, 55–80. [CrossRef]
41. Larson, A.C.; von Dreele, R.B. General Structure Analysis System (GSAS). In *Los Alamos National Laboratory Report LAUR*; The Regents of the University of California: Oakland, CA, USA, 2000; pp. 86–748.
42. Toby, B.H. *EXPGUI*, a Graphical User Interface for *GSAS*. *J. Appl. Crystallogr.* **2001**, *34*, 210–213. [CrossRef]
43. Rodríguez-Carvajal, J. Recent Advances in Magnetic Structure Determination by Neutron Powder Diffraction. *Physica B Condens. Matter* **1993**, *192*, 55–69. [CrossRef]
44. Hirao, N.; Kawaguchi, S.I.; Hirose, K.; Shimizu, K.; Ohtani, E.; Ohishi, Y. New developments in high-pressure X-ray diffraction beamline for diamond anvil cell at SPring-8. *Matter Radiat. Extrem.* **2020**, *5*, 018403. [CrossRef]
45. Seto, Y.; Nishio-Hamane, D.; Nagai, T.; Sata, N. Development of a software suite on X-ray diffraction experiments. *Rev. High Press. Sci. Technol.* **2010**, *20*, 269–276. [CrossRef]
46. Sakai, T.; Yagi, T.; Ohfuji, H.; Irifune, T.; Ohishi, Y.; Hirao, N.; Suzuki, Y.; Kuroda, Y.; Asakawa, T.; Kanemura, T. High-pressure generation using double stage micro-paired diamond anvils shaped by focused ion beam. *Rev. Sci. Instrum.* **2015**, *86*, 033905. [CrossRef] [PubMed]
47. Sakai, T.; Yagi, T.; Irifune, T.; Kadobayashi, H.; Hirao, N.; Kunimoto, T.; Ohfuji, H.; Kawaguchi-Imada, S.; Ohishi, Y.; Tateno, S.; et al. High pressure generation using double-stage diamond anvil technique: Problems and equations of state of rhenium. *High Press. Res.* **2018**, *38*, 107–119. [CrossRef]
48. Zha, C.-S.; Mao, H.-K.; Hemley, R.J. Elasticity of MgO and a Primary Pressure Scale to 55 GPa. *Proc. Natl. Acad. Sci. USA* **2000**, *97*, 13494. [CrossRef]
49. Klotz, S.; Chervin, J.C.; Munsch, P.; Le Marchand, G. Hydrostatic limits of 11 pressure transmitting media. *J. Phys. D Appl. Phys.* **2009**, *42*, 075413. [CrossRef]